Competition–dispersal tradeoff ecologically differentiates recently speciated marine bacterioplankton populations

Yutaka Yawata[1], Otto X. Cordero, Filippo Menolascina, Jan-Hendrik Hehemann, Martin F. Polz, and Roman Stocker[1]

Ralph M. Parsons Laboratory, Department of Civil and Environmental Engineering, Massachusetts Institute of Technology, Cambridge, MA 02139

Edited by Tom M. Fenchel, University of Copenhagen, Helsingor, Denmark, and approved February 6, 2014 (received for review October 9, 2013)

Although competition–dispersal tradeoffs are commonly invoked to explain species coexistence for animals and plants in spatially structured environments, such mechanisms for coexistence remain unknown for microorganisms. Here we show that two recently speciated marine bacterioplankton populations pursue different behavioral strategies to exploit nutrient particles in adaptation to the landscape of ephemeral nutrient patches characteristic of ocean water. These differences are mediated primarily by differential colonization of and dispersal among particles. Whereas one population is specialized to colonize particles by attaching and growing biofilms, the other is specialized to disperse among particles by rapidly detecting and swimming toward new particles, implying that it can better exploit short-lived patches. Because the two populations are very similar in their genomic composition, metabolic abilities, chemotactic sensitivity, and swimming speed, this fine-scale behavioral adaptation may have been responsible for the onset of the ecological differentiation between them. These results demonstrate that the principles of spatial ecology, traditionally applied at macroscales, can be extended to the ocean's microscale to understand how the rich spatiotemporal structure of the resource landscape contributes to the fine-scale ecological differentiation and species coexistence among marine bacteria.

migration | attachment | fugitive species | microfluidics | marine particles

Spatially structured environments allow species with similar resource preferences to coexist by modulating their propensity to thoroughly exploit patches versus dispersing to find new patches, trading off their ability to access resources at local versus global scales (1–4). This fundamental ecological principle offers an attractive explanation for the genetic diversity of microbial communities, which often inhabit environments that are seemingly homogeneous but in fact highly structured at the microscale. In the ocean, for example, strong heterogeneity at the micrometer scale stems from a broad range of sources, including phytoplankton exudates, cell lysis, and excretions by larger organisms (5, 6). These different forms of organic matter are spatially localized and are important nutrient sources for bacterioplankton (7). The fact that the microscale marine landscape is composed of discrete resource patches at time and length scales commensurate with bacterial dispersal suggests the exciting possibility that theories developed in the context of landscape ecology (2, 8, 9) could be applied to understand the enormous diversity of microorganisms inhabiting the ocean's water column.

One of the best-studied phenomena in spatial ecology is the tradeoff between competition and dispersal (9–11), where species with an inferior ability to use resources can compensate by migrating more frequently and over longer distances, adopting what are called "fugitive" strategies (12). Whereas superior competitors dominate within patches, fugitive strategists gain an edge through the discovery and early colonization of fresh resource patches (10, 11). The inverse relationship between competitive ability on a resource patch and readiness to colonize new patches has been found to explain the coexistence of ant species on plants (4), in host–parasitoid systems (1), and in artificial bacterial communities (13, 14). However, a basic tenet of microbial ecology is that in nature, small organisms such as bacteria are dispersed passively and their distribution is homogenized across macroscales (15). Thus, it remains unclear whether the ocean's microscale spatial landscape can sustain ecological differentiation of natural microbial populations, or whether such differentiation is explained solely by niche partitioning at the level of resource preferences and abiotic conditions (16, 17).

Here we ask whether and how differential interaction with microscale nutrient particles and gradients can underpin the ecological differentiation of two recently diverged, sympatric populations of *Vibrio cyclitrophicus*. Genomic analysis of these populations has revealed that they are in the early stages of genetic differentiation, with most of the genome still showing evidence of previously unrestricted recombination among members of the parental populations whereas the most recent recombination events already show specificity for the nascent sister populations (18). The genetic differentiation, although small, seems to have ecological implications because these two populations have been retrieved from different microenvironments in the water column, namely large particles (>64 μm; L population) versus bulk fluid and small particles (<5 μm; S population) (16). That this results from a stable ecological distinction is suggested by recurrent observation of the two populations in the same size fractions in subsequent years (19). We probed the spectrum of spatial behaviors of 12 isolates of *V. cyclitrophicus* using microfluidic models of microscale resource landscapes to understand the behavioral mechanisms

Significance

The resource landscape for marine microbes is composed of microscale resource patches, but whether this microheterogeneity can drive the ecological differentiation of natural microbial populations remains unclear. The tradeoff between two nascent populations of marine bacteria demonstrated here is significant for several reasons. First, it illustrates that principles of spatial ecology, so far only illustrated for animals and plants, apply to the ephemeral, microscale nutrient landscape of marine microbes. Second, the results suggest that differential behavior can ensure coexistence of otherwise very similar populations of organisms. Finally, because the demonstrated tradeoff induces microgeographic separation among the populations, it may be a crucial step in initiating gene flow barriers that ultimately allow the populations to embark on differential evolutionary trajectories.

Author contributions: Y.Y., O.X.C., M.F.P., and R.S. designed research; Y.Y. and F.M. performed research; Y.Y. and J.-H.H. contributed new reagents/analytic tools; Y.Y., O.X.C., and F.M. analyzed data; and Y.Y., O.X.C., M.F.P., and R.S. wrote the paper.

The authors declare no conflict of interest.

This article is a PNAS Direct Submission.

[1]To whom correspondence may be addressed. E-mail: yyawata@mit.edu or romans@mit.edu.

This article contains supporting information online at www.pnas.org/lookup/suppl/doi:10.1073/pnas.1318943111/-/DCSupplemental.

underpinning their niche partitioning and the ecological tradeoff enabling their coexistence.

We demonstrate that the two *V. cyclitrophicus* populations have different ecological strategies to interact with microscale nutrient patches in the ocean. We show that the superior ability of the particle-attaching L population to colocalize with the highest nutrient concentrations is offset by the ability of the nonattaching S population to rapidly migrate to new nutrient sources upon a temporal change in the nutrient landscape. These results reveal that the ecological differentiation of the two sympatric populations is driven by a competition–dispersal tradeoff, whereby exploitation of individual nutrient patches comes at the cost of a reduced ability to migrate toward new patches. The ephemeral nature of marine microscale nutrient patches thus enables the coexistence of two foraging strategies, respectively favoring high access to resources at the individual patch level and at the microscale landscape level.

Results and Discussion

We began our systematic comparison of spatial behavioral adaptations by measuring the ability of the two populations to attach to and colonize surfaces, motivated by the predominant occurrence of the L and S populations in the large-particle fraction and the free-living fraction of seawater samples, respectively (16). Attachment to surfaces is a widespread phenotype of marine bacteria (20), used to associate with particles and hosts (21–23), and a genomic comparison of the two populations suggested differential genetic potential for attachment (18).

We found strong and widespread differences in the attachment behavior of seven L and five S isolates, respectively. Imaging of attachment to polystyrene over 1 h (*SI Materials and Methods*) yielded a ratio, α, of 4.9 between the numbers of attached cells for L- (695 ± 161 cells per mm^2) and S-population isolates (143 ± 59 cells per mm^2) (Fig. 1*A*). The attachment ratio was even larger (α = 42.4) when the surface was more hydrophobic (Fig. S1*A*), and only mildly smaller (α = 4.4) when it was more hydrophilic. We measured similar differences in attachment to surfaces made of the polysaccharides found in the cell walls of algae and phytoplankton, specifically agarose (α = 11.4; Fig. S1*B*), cellulose (α = 4.5; Fig. S1*B*), and alginate (α = 14.9; Fig. S1*C*), although not with chitin (Fig. S1*C* and *SI Results and Discussion*). These results reveal a first, clear behavioral difference between the two populations, verifying the original hypothesis based on dissimilar distribution in the wild (18) that attachment to particles is an important mechanism in their ecological differentiation, and further demonstrating that differences in attachment strategies are largely independent of the precise chemical state of particles.

The different preference for surfaces was further manifest in the ability of the L population but not the S population to rapidly form biofilms and thus stably associate with surfaces (Fig. 1 *B* and *C* and Fig. S1*D*). Biofilm formation, through the production of extracellular polymers that cement and protect cells, is a common bacterial behavior for the long-term colonization of surfaces (24, 25). Experiments under batch culture conditions showed that L-population isolates exhibited approximately ninefold higher values of area coverage than S-population isolates after 5 h, and this difference remained consistent throughout the early stages of biofilm formation (Fig. 1*B*). After 3 d, the S-population isolate 1F111 hardly formed any biofilm, whereas the L-population isolate ZF270 formed a dense biofilm (Fig. 1*C*). Staining with an FITC-labeled lectin confirmed the biofilm nature of this cell assemblage by revealing the presence of a rich extracellular matrix (Fig. S1*D*). Even the precolonization of a surface by an isolate from the L population (ZF270) did not reduce the difference in surface colonization among isolates from the two populations (Fig. S1*E*).

These behavioral differentiations in surface colonization are supported by both genomic and phenotypic evidence. Genomic analysis has shown that only a small number of gene clusters are specific to either population (18). All isolates from the L population but none from the S population harbor the mannose sensitive hemagglutinin (*msh*) gene cluster (18) (Fig. 1*D*), which encodes the mannose-sensitive hemagglutinin type IV pili and is involved in the surface attachment of *Vibrio cholerae* (26). The differential presence of the *msh* gene cluster exactly matches the difference in surface attachment between the two populations (Fig. 1*A* and Fig. S1 *A–C* and *E*) and is further confirmed at the phenotypic level: By imaging 25 cells from two isolates per population via electron microscopy, we found that pili are present in 84–91% of cells from the L population and in 0% of cells from the S population (Fig. 1*E*). A second gene cluster

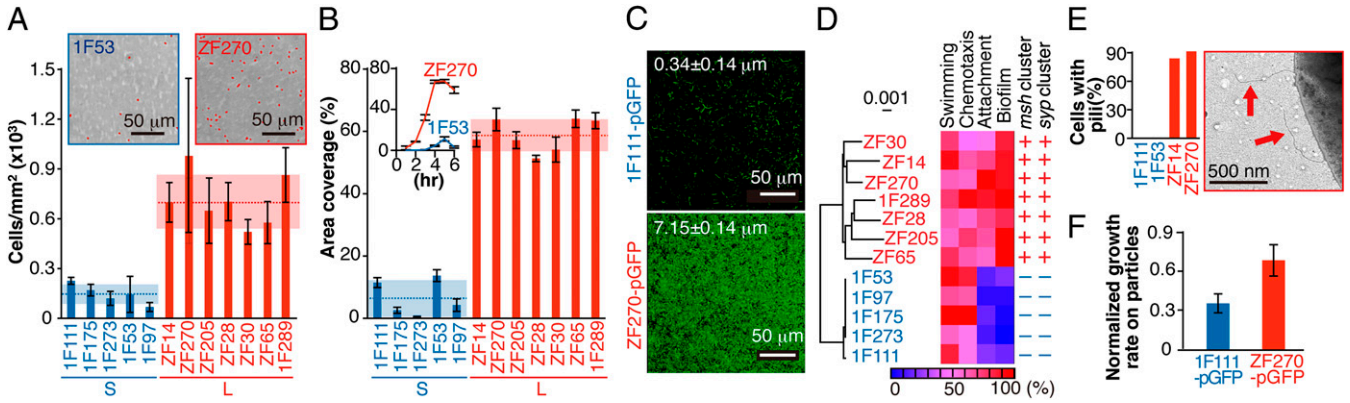

Fig. 1. Surface attachment and biofilm formation differ considerably between two closely related genetic populations of *V. cyclitrophicus*. (*A*) Attachment to a polystyrene surface (45° contact angle) after 1 h for each of five isolates from the S population (S) and seven from the L population (L). (*Inset*) Phase–contrast image of attached cells (red). Dashed lines and shadings denote averages and SDs for each population. (*B*) Percent surface coverage after 5 h for the 12 isolates. (*Inset*) Time course of surface coverage for one S (blue) and one L (red) isolate. Dashed lines and shadings denote averages and SDs for each population. (*C*) Three-day-old biofilms, imaged by confocal microscopy, for one S (blue) and one L (red) isolate, both GFP-tagged. Numbers denote biofilm thickness (mean ± SD; $n = 3$). (*D*) Correlation among lineage, phenotypic traits, and gene content. The table shows the phylogenetic tree, relative magnitude (color-coded) of swimming, chemotaxis to serine, surface attachment, biofilm formation, and the presence (+) or absence (–) of gene clusters. (*E*) Percentage of cells with pili, calculated from transmission electron microscopy (TEM) images of 25 cells per isolate. The average number of pili of L-population isolates was 2.2 ± 0.9 (ZF14) and 1.7 ± 1.2 (ZF270), whereas no S cell had any pili. A TEM image of isolate ZF14, with arrows indicating pili. (*F*) Growth rate for one S (blue) and one L (red) isolate, with alginate particles as the sole carbon source, normalized by the growth rate with the same total amount of soluble alginate. Data are averages of three independent experiments, and error bars denote SDs.

harbored only by the L population is the symbiosis polysaccharide (*syp*) cluster (18) (Fig. 1*D*), which is involved in the production of extracellular matrix in *Vibrio fischerii* (27). Its differential presence matches the superior ability of the L population to form biofilms (Fig. 1 *B* and *C* and Fig. S1*D*). Among all population-specific genes that have been reported for these two populations (18), the only genes potentially related to attachment are those in the *msh* and *syp* clusters. The specificity of the *msh* and *syp* gene clusters, together with their known functions in other *Vibrio* species, suggests that they play a fundamental role in regulating the different habitat preferences between the two *V. cyclitrophicus* populations.

In the ocean, particles are nutritional hotspots in an otherwise nutrient-poor water column, and considerably increase uptake rates of attached bacteria (28). Our observations of differential attachment then imply a competitive advantage for the L population, owing to its superior ability to colocalize with the high nutrient concentrations occurring on particles. We verified this hypothesis by quantifying growth on alginate as the sole carbon source: We provided cells the same total amount of alginate in either particulate or dissolved form, and compared their growth rate on the two forms of alginate to isolate the effect of the physical interaction with particles. Having resources concentrated on particles generally decreases the rate of nutrient exposure per cell compared with the case of uniformly dissolved nutrients. This spatial localization of resources had a much stronger negative impact on the S-population isolate 1F111, whose drop in growth rate on particulate alginate relative to dissolved alginate was more than twofold larger compared with the L-population isolate ZF270 (Fig. 1*F*), which was able to compensate by attaching to and colocalizing with the particles. This result confirms the hypothesis that attachment confers a growth advantage to cells from the L population and shows how the physical interaction between bacteria and particles has a considerable effect on growth.

What tradeoff, then, prevents the S population from being outcompeted? We hypothesized that the two populations differ in their ability to swim or respond to chemical gradients (chemotaxis), two widespread phenotypes in the ocean, where they allow bacteria to locate and exploit microscale nutrient patches (6, 7, 29). Specifically, we expected that the S population would have superior motility and chemotaxis to compensate for the disadvantage in attachment. However, detailed analysis of traditionally measured behavioral abilities—swimming speed and chemotactic preferences—yielded highly comparable responses for the two populations. Instead, a microfluidic system quantifying the response to temporal shifts in the nutrient landscape revealed a strong difference between L and S isolates, showing that the tradeoff between the two populations does not occur at the level of an individual patch but rather resides in the differentiation between a strategy that maximizes access to resources at the patch level (L population) and one that favors access to resources at the landscape level (S population). In the following, we demonstrate these results.

Cell tracking (*SI Materials and Methods*) showed that all 12 isolates exhibited comparable swimming speeds, averaging 59 ± 12 μm/s (S) and 54 ± 9 μm/s (L) (Fig. 2*A*). Additional measurements for S-isolate 1F53 and L-isolate ZF270 further showed that cell size and flagellation are comparable (Fig. 2*A*) and that the similarity in swimming speed is independent of the growth stage (Fig. 2*A*, *Inset*).

Chemotaxis toward steady resource gradients, generated by diffusion within microfluidic devices (design 1; Fig. S2), also revealed no significant difference between the two populations. This can be seen from the spatial distribution of cells for each of the 12 isolates along a gradient of the amino acid serine (Fig. 2 *B* and *C*). A quantitative comparison of the chemotaxis magnitude, defined as the skewness of the cell distribution (Fig. 2*D*), yielded values of 1.1 ± 0.3 (S) and 1.0 ± 0.2 (L). An in-depth comparison between S-isolate 1F53 and L-isolate ZF28 showed comparable chemotaxis also toward other important marine chemoattractants (Fig. 2*E*), including glucose, a product of photosynthesis by phytoplankton (30); *N*-acetyl glucosamine (GlcNAc), the monomer of the chitin exoskeleton of many marine organisms (31); and dimethylsulfoniopropionate (DMSP), a climatically important sulfur compound that serves a broad range of physiological and signaling functions in the ocean (32). Although we cannot rule out differences in the chemotactic preferences for other chemical compounds, these observations strongly suggest that the S population does not outperform the L population in terms of swimming ability and chemotactic responses to steady resource gradients.

Taken together, the results on attachment and motility imply that the tradeoff enabling the coexistence of the two populations cannot be understood at the single-patch level. Instead, the stable surface colonization by the L population together with the transient nature of resource hotspots in the ocean, where lysis (33), sloppy feeding (34), particle sinking (34), and turbulent stirring (29) all result in ephemeral patches of dissolved organic matter (35–37), led us to hypothesize that the S population gains its competitive advantage at the microscale landscape level by exploiting the temporal variability of the resource landscape and the continuous appearance of new patches. Specifically, we tested the hypothesis that S cells can better respond to a temporal change in the resource landscape. We first generated a steady resource gradient by releasing serine from the porous

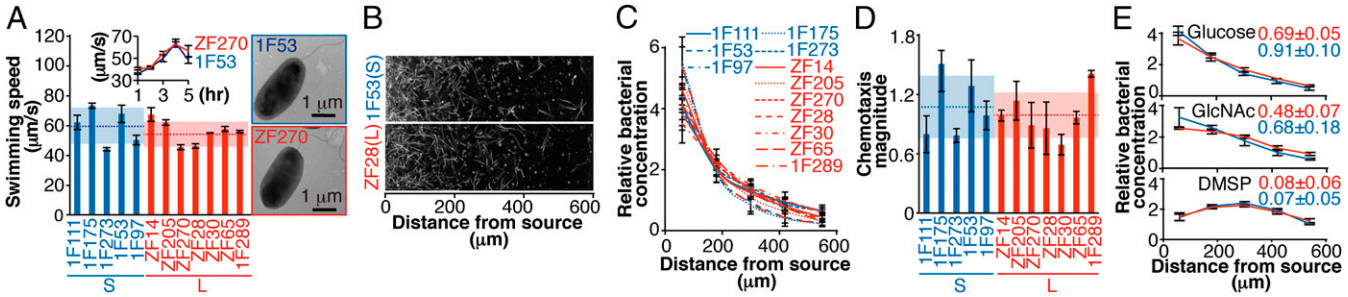

Fig. 2. Motility and chemotaxis are very similar for the two genetic populations of *V. cyclitrophicus*. (*A*) Swimming speed of the 12 isolates from the S (blue) and L (red) populations, measured at mid-exponential phase. Dashed lines and shadings denote averages and SDs for each population. (*Inset*) Growth-stage dependence of speed for one S (blue) and one L (red) isolate, whose cell shape is shown in the TEM images. (*B*) Swimming trajectories (white) in a steady, linear serine concentration profile for one S (blue) and one L (red) isolate. (*C*) Bacterial distribution along a serine gradient, quantified as the relative concentration of cells vs. distance from the serine source ($x = 0$). (*D*) Magnitude of chemotaxis toward serine, quantified as the skewness of the bacterial distributions in *C*. Dashed lines and shadings denote averages and SDs for each population. (*E*) Bacterial distribution in gradients of D-glucose, GlcNAc, and DMSP for one S (blue) and one L (red) isolate. Numbers denote chemotaxis magnitude. In all panels (except *B*), data are averages over three experiments, and error bars denote SDs.

sidewall of a microfluidic device (design 2; Figs. S3 and S4), whereupon cells from both populations (isolates 1F111 and ZF270) rapidly (<3 min) migrated toward the serine-releasing surface (Fig. 3*A*). After 10 min, we switched the serine release to the opposite sidewall, thus inverting the direction of the gradient. Strikingly, only the S isolate (1F111) responded to the change, by migrating toward the new nutrient-rich surface within <10 min (Fig. 3 *B* and *C* and Movie S1). In contrast, the L isolate (ZF270) remained attached to the original surface (for at least 30 min; Fig. 3*C*), despite the considerable nutritional impoverishment of that surface. Additional experiments with a device that allowed quantification of attachment in the presence of chemical gradients confirmed the differential behavior of the two populations (Figs. S5–S8 and *SI Results and Discussion*).

The steady attachment to particles thus creates a tradeoff between resource accessibility at the patch and landscape levels. Because of their stable attachment to particles, L cells have higher access to resources at the patch level. However, this comes to the detriment of their migration ability in response to temporal changes in nutrient availability, which limits their access to resources at the microscale landscape level. In contrast, S cells do not commit to surfaces by attachment and biofilm formation—reducing their growth rate on particles compared with L cells (Fig. 1*F*)—but are continuously ready to migrate to new patches. Thus, the L and S populations differ in their ecological strategies for resource utilization, with the L population being better at accessing localized resources at the individual patch level and the S population being better at dispersing and discovering new patches. The result is a tradeoff between competition and dispersal (1, 4, 9–11, 14) that we expect favors either population depending on the spatiotemporal particle dynamics in the environment: Whereas the L population benefits from long-lived particles where steady attachment yields a competitive advantage (Fig. 1*F*), the S population benefits from high rates of particle turnover where frequent migration is advantageous (38, 39).

Our finding thus provides a new interpretation of the predominance of S and L populations in different size fractions of the marine water column (16, 18): Prevalent occurrence in small size fractions does not imply habitat specialization toward bulk water conditions but rather propensity to migration among hotspots over particle attachment. Furthermore, the ecological tradeoff we identified provides a simple explanation for coexistence even if populations fully overlap in their metabolic preferences, and indeed both the gene content and a Biolog assay suggest strong metabolic similarity between the two populations (Fig. S9 and *SI Results and Discussion*). Finally, a different experimental system capable of producing and renewing surfaces and gradients over several generations will be required to directly test coexistence, something that was not possible in our microfluidic devices. Such a system will further reveal the role of environmental conditions (concentration and composition of particles, rate of occurrence of new particles, particle size, duration of chemical release from a particle) in the outcome of the coexistence and relative prevalence of each population.

The systematic analysis of a broad spectrum of spatial behaviors suggests a model for the ecological and evolutionary differentiation between the two populations of *V. cyclitrophicus* (Fig. 4). Isolates from the L population find particles by chemotaxis, attach, and establish a steady association with them by building biofilms. This affords them access to the highest

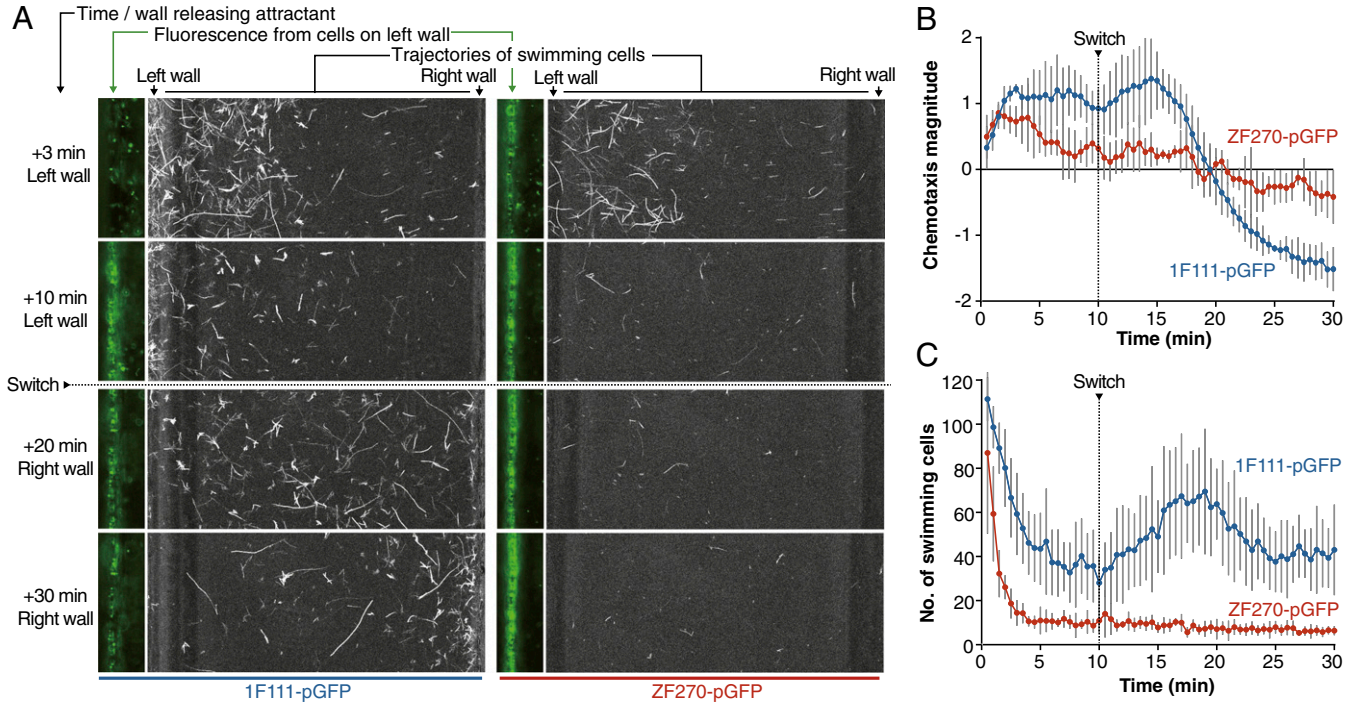

Fig. 3. Only the S population can rapidly respond to a temporal change in nutrient conditions. (*A*) Behavioral response of one S (blue) and one L (red) isolate in a temporally varying nutrient landscape. Large panels show swimming trajectories; small panels show the region close to the left sidewall, from which serine was released for the first 10 min. (*B*) Time course of the chemotaxis magnitude (as in Fig. 2*D*). Positive values of the chemotaxis magnitude indicate attraction towards the left side of the channel; negative values indicate attraction towards the right side of the channel. Because surface-attached cells are not included when quantifying chemotaxis, the magnitude of chemotaxis of the L population here is lower than in Fig. 2*D*, due to the strong attachment of the L population to the agarose sidewalls of the test channel in the design 2 device (Fig. S3) used here, compared with the PDMS sidewalls in the design 1 device (Fig. S2) used to obtain Fig. 2*D*. (*C*) Time course of the number of cells swimming in the bulk (>5 μm from either sidewall). The decrease for the S population around 10 and 30 min was due to cells hovering adjacent to the (serine-releasing) sidewalls, where cell tracking is hindered by optical reflections (*SI Results and Discussion*). The dashed line indicates when the direction of the attractant gradient was switched. Data are averages from four experiments and error bars denote SDs.

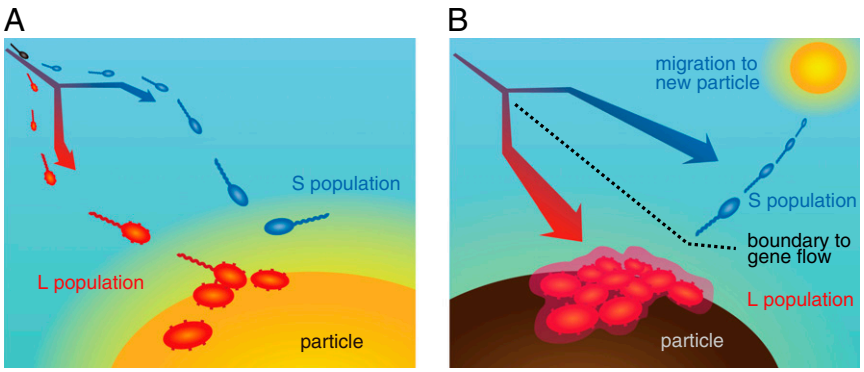

Fig. 4. Model for the tradeoff between the behavioral adaptations of the two *V. cyclitrophicus* populations. (*A*) Both populations swim and respond to chemical gradients, but only the L population attaches and forms biofilms on particles, whereas the S population hovers near the surface. (*B*) When a more nutrient-rich particle appears nearby, only the S population is ready to rapidly respond by migrating to the new source.

nutrient concentrations: They are the first line of consumption of dissolved nutrients generated in the particle [e.g., by enzymatic processes (40)], making them strong competitors on these nutrient patches. In contrast, isolates from the S population find nutrient hotspots, including particles, by chemotaxis, but only associate with particles loosely by hovering in close proximity to their surface, without settling. Although this puts them in "second row" in terms of access to particle-originated nutrients, it buys them the flexibility to rapidly respond to new hotspots, for example when nutrients on the particle dwindle or a stronger hotspot appears nearby. We note that, beyond this fundamental differentiation in ecological strategies, coexistence can further be driven by other side effects of spatial partitioning, such as less-direct competition for resources between the S and L populations and different mortality rates due to higher preference of predators for particles. Additionally, a population-specific allele sweep in the *rpoS2* sigma factor gene previously detected (18) may complement niche adaptation by mediating differential responses to stress.

These different ecological strategies could contribute to reduce recombination between populations, promoting sympatric genetic differentiation and lineage diversion and explaining the gene flow boundary previously reported (16, 18). The origin of this gene flow boundary is thus considerably subtler than expected, because it does not require metabolic differentiation and operates only through differential propensity for attachment to particles and dissociation from nutrient hotspots. Given the ease with which these behavioral differences could evolve, for example by horizontal gene transfer of the *msh* or *syp* gene clusters, we propose that this bifurcation of spatial behaviors drove the early stages of population differentiation in *V. cyclitrophicus*. This work, then, provides a blueprint for connecting behavioral adaptations with microbial diversity and highlights how subtle a difference in spatial behavior can be sufficient to curtail gene flow among populations, and how important the spatial and temporal signatures of the marine microscale nutrient landscape are for microbial diversification in the ocean.

Materials and Methods

Microfluidic Devices. Two different versions of the microfluidic gradient generator, modified from ref. 41, were used in the chemotaxis experiments with steady linear concentration profiles (design 1; Fig. S2*A*; results in Fig. 2) and time-varying concentration profiles (design 2; Fig. S3*A*; results in Fig. 3). Design 1 corresponds to design 1 in ref. 41, whereas design 2 is a variant on the same design principle. Both gradient generators are made of three layers: a polydimethylsiloxane (PDMS) layer on top (impermeable to solutes), an agarose layer in the middle (permeable to solutes), and a glass slide at the bottom (for support). The design concept consists of fabricating microchannels within the layer of PDMS (Sylgard 184; Dow Corning) and/or the layer of agarose (Ultra Pure Agarose; Invitrogen) to establish chemoattractant gradients by diffusion (Figs. S2 and S3). PDMS channels were designed using CAD software (Autodesk) and printed onto transparency film with a high-resolution image setter (Fineline Imaging). For details on fabrication and operation of microfluidic devices, see *SI Materials and Methods*.

Cell Tracking Within Concentration Gradients. Cells were imaged in phase contrast using a 10× (N.A. 0.30) or 20× (N.A. 0.45) objective by acquiring sequences of 200 frames (movies) at 50 frames per s with a CCD camera (PCO 1600; Cooke; 1,600 × 1,200 pixels). The field of view was 0.9 × 1.2 mm with the 10× objective and 0.45 × 0.6 mm with the 20× objective. Swimming trajectories were obtained from each movie by locating the maximum pixel intensity for each pixel over the duration of the movie. We performed image analysis by subtracting each frame from the following one, to focus only on motile cells, and by subsequently locating bacteria in each frame as peaks in a monochrome intensity field, using IPLab (Scanalytics). Bacterial positions were determined over all frames in a movie and binned to yield the relative bacterial concentration profile, as a function of the distance from the sidewall of the test chamber with the highest chemoattractant concentration, using custom MATLAB (The MathWorks) routines.

Chemotaxis in Steady, Linear Chemoattractant Profiles. Design 1 (Fig. S2*A*) among the microfluidic gradient generators was used for the chemotaxis assays under steady linear profiles of chemoattractant concentration. In this design, the irrigation channels and the test channel are all located within the PDMS layer. By continuously flowing chemoattractant in one of the two irrigation channels and filtered autoclaved seawater in the other and relying on diffusion of the chemoattractant into the underlying agarose layer, this device produces a steady, linear concentration profile within the underlying agarose layer (41). By diffusion, this linear chemoattractant profile also extends into the cell suspension within the test channel (Fig. S2*B*). After >10 min, a time sufficient to ensure the establishment of the linear gradient (41), we injected mid–exponential-phase cells (OD_{600} 0.5) into the test channel, thus exposing them to the linear chemoattractant profile. Cells were tracked as described above, yielding the distribution of cells along the width of the test channel (i.e., along the chemoattractant gradient). The chemotaxis magnitude was measured by computing the skewness of the cell distribution. We used L-serine, D-glucose, *N*-acetyl D-glucosamine (GlcNAc), and dimethylsulfoniopropionate (DMSP) as chemoattractants, each at a concentration of 50 μM. Chemotaxis assays with L-serine were performed for all 12 isolates in Table S1, whereas those with D-glucose, GlcNAc, and DMSP were performed with 1 isolate from each population (1F53 and ZF28). Three independent experiments were performed in each case.

Bacterial Behavior Under Time-Varying Nutrient Conditions. Design 2 (Fig. S3*A*) among the microfluidic gradient generators was used to study bacterial behavior under time-varying nutrient conditions. In this design, only the irrigation channels were located in the PDMS layer, whereas the test channel was in the agarose layer. As in design 1, we created a linear concentration profile within the agarose layer by continuously flowing chemoattractant in one of the two irrigation channels and filtered autoclaved seawater in the other. This time, however, chemoattractant diffused into the test channel through the sidewalls (not the bottom surface) of the test channel (Fig. S3*B*). In this fashion, the agarose sidewall serves as a model for the surface of a nutrient particle, which releases chemicals and can be colonized by bacteria (Fig. 3 and Fig. S3*B*). Mid–exponential-phase cells (OD_{600} 0.4) were diluted to

OD_{600} 0.04 with filtered autoclaved seawater and introduced into the test channel after >10 min from the start of the flow in the irrigation channels to ensure establishment of the gradient. To model a temporal change in the nutrient conditions, 10 min after injecting cells into the test channel, we reversed the direction of the chemoattractant gradient by swapping the flows in the two irrigation channels (i.e., swapping chemoattractant and filtered autoclaved seawater), so that chemoattractant began to enter the test channel from the surface of the opposite sidewall. Fig. S4 shows the results of a numerical model (*SI Materials and Methods*) of the time course of the chemoattractant concentration field in the agarose layer and in the test channel, illustrating each of the steps described above. Throughout the experiment, quantification of the cells' swimming response was performed by video microscopy, as described above. Furthermore, we imaged the association of cells (which expressed GFP) with the agarose sidewall surfaces by epifluorescence microscopy using a mercury lamp (X-Cite 120Q; Lumen Dynamics), a 440–480 nm band-pass filter for excitation, and a 535–550 nm band-pass filter for emission. Experiments were performed with two isolates (1F111-pGFP and ZF270-pGFP) that harbor the GFP-expressing vector pGFP (Table S1), with four independent experiments per isolate (Fig. 3).

Growth-Rate Comparison. Growth on alginate as the sole carbon source was quantified by providing cells with the same total amount of alginate in either particulate (*SI Materials and Methods*) or dissolved form and comparing the growth rates of isolates on the two forms of alginate. The growth rate (Fig. 1*F*) of one S (1F111-pGFP) and one L (ZF270-pGFP) isolate was tested in this manner. A mid–exponential-phase culture (OD_{600} 0.5) was washed with fresh medium and diluted to ~3.0×10^5 CFU/mL in minimal medium containing 0.001% (wt/vol) of alginate in soluble or particulate form as the sole carbon source. A 300-μL aliquot was introduced into a test tube and incubated at 30 °C for 13 h. Ten-microliter aliquots were sampled at the start and end of experiments to determine CFU by plate counting, and the number of divisions per hour was then calculated. The minimal medium for these experiments was prepared as previously described (42), with omission of EDTA and addition of a vitamin mix (43). Experiments were performed in triplicate.

Other Methods. Methods describing bacterial isolates, cell-culture protocols, microfabrication, surface-attachment assays, biofilm experiments, swimming-speed measurements, genetic analysis, and substrate-utilization analysis are described in *SI Materials and Methods*.

ACKNOWLEDGMENTS. We thank Katharina Ribbeck for access to confocal microscopy; Arne Heydorn for providing COMSTAT; and Marino Gatto, Renato Casagrandi, and Melissa Garren for comments. Y.Y. was partially supported by the Japanese Society for the Promotion of Science. We acknowledge support from National Science Foundation Grant OCE-0744641-CAREER (to R.S.), National Institutes of Health Grant 1R01GM100473-01 (to R.S.), and Gordon and Betty Moore Microbial Initiative Investigator Award no. 3783 (to R.S.).

1. Lei G, Hanski I (1998) Spatial dynamics of two competing specialist parasitoids in a host metapopulation. *J Anim Ecol* 67(3):422–433.
2. Tilman D (1994) Competition and biodiversity in spatially structured habitats. *Ecology* 75(1):2–16.
3. Rainey PB, Travisano M (1998) Adaptive radiation in a heterogeneous environment. *Nature* 394(6688):69–72.
4. Yu DW, Wilson HB, Pierce NE (2001) An empirical model of species coexistence in a spatially structured environment. *Ecology* 82(6):1761–1771.
5. Azam F, Malfatti F (2007) Microbial structuring of marine ecosystems. *Nat Rev Microbiol* 5(10):782–791.
6. Stocker R (2012) Marine microbes see a sea of gradients. *Science* 338(6107):628–633.
7. Stocker R, Seymour JR, Samadani A, Hunt DE, Polz MF (2008) Rapid chemotactic response enables marine bacteria to exploit ephemeral microscale nutrient patches. *Proc Natl Acad Sci USA* 105(11):4209–4214.
8. Amarasekare P (2003) Competitive coexistence in spatially structured environments: A synthesis. *Ecol Lett* 6(12):1109–1122.
9. Levins R, Culver D (1971) Regional coexistence of species and competition between rare species. *Proc Natl Acad Sci USA* 68(6):1246–1248.
10. Hastings A (1980) Disturbance, coexistence, history, and competition for space. *Theor Popul Biol* 18(3):363–373.
11. Nee S, May RM (1992) Dynamics of metapopulations: Habitat destruction and competitive coexistence. *J Anim Ecol* 61(1):37–40.
12. Bolker BM, Pacala SW (1999) Spatial moment equations for plant competition: Understanding spatial strategies and the advantages of short dispersal. *Am Nat* 153(6):575–602.
13. Livingston G, et al. (2012) Competition-colonization dynamics in experimental bacterial metacommunities. *Nat Commun* 3: Article 1234.
14. Nadell CD, Bassler BL (2011) A fitness trade-off between local competition and dispersal in *Vibrio cholerae* biofilms. *Proc Natl Acad Sci USA* 108(34):14181–14185.
15. Baas-Becking LGM (1934) [*Geobiologie of Inleiding tot de Milieukunde*] (W. P. Van Stockum & Zoon, The Hague).
16. Hunt DE, et al. (2008) Resource partitioning and sympatric differentiation among closely related bacterioplankton. *Science* 320(5879):1081–1085.
17. Johnson ZI, et al. (2006) Niche partitioning among *Prochlorococcus* ecotypes along ocean-scale environmental gradients. *Science* 311(5768):1737–1740.
18. Shapiro BJ, et al. (2012) Population genomics of early events in the ecological differentiation of bacteria. *Science* 336(6077):48–51.
19. Szabo G, et al. (2013) Reproducibility of *Vibrionaceae* population structure in coastal bacterioplankton. *ISME J* 7(3):509–519.
20. Petrova OE, Sauer K (2012) Sticky situations: Key components that control bacterial surface attachment. *J Bacteriol* 194(10):2413–2425.
21. Grossart HP, Kiørboe T, Tang K, Ploug H (2003) Bacterial colonization of particles: Growth and interactions. *Appl Environ Microbiol* 69(6):3500–3509.
22. Sonnenschein EC, Syit DA, Grossart HP, Ullrich MS (2012) Chemotaxis of *Marinobacter adhaerens* and its impact on attachment to the diatom *Thalassiosira weissflogii*. *Appl Environ Microbiol* 78(19):6900–6907.
23. Kiørboe T, Tang K, Grossart HP, Ploug H (2003) Dynamics of microbial communities on marine snow aggregates: Colonization, growth, detachment, and grazing mortality of attached bacteria. *Appl Environ Microbiol* 69(6):3036–3047.
24. Hall-Stoodley L, Costerton JW, Stoodley P (2004) Bacterial biofilms: From the natural environment to infectious diseases. *Nat Rev Microbiol* 2(2):95–108.
25. Stoodley P, Sauer K, Davies DG, Costerton JW (2002) Biofilms as complex differentiated communities. *Annu Rev Microbiol* 56(2):187–209.
26. Meibom KL, et al. (2004) The *Vibrio cholerae* chitin utilization program. *Proc Natl Acad Sci USA* 101(8):2524–2529.
27. Shibata S, Yip ES, Quirke KP, Ondrey JM, Visick KL (2012) Roles of the structural symbiosis polysaccharide (*syp*) genes in host colonization, biofilm formation, and polysaccharide biosynthesis in *Vibrio fischeri*. *J Bacteriol* 194(24):6736–6747.
28. Ayo B, et al. (2001) Kinetics of glucose and amino acid uptake by attached and free-living marine bacteria in oligotrophic waters. *Mar Biol* 138(5):1071–1076.
29. Taylor JR, Stocker R (2012) Trade-offs of chemotactic foraging in turbulent water. *Science* 338(6107):675–679.
30. Hama T, Yanagi K (2001) Production and neutral aldose composition of dissolved carbohydrates excreted by natural marine phytoplankton populations. *Limnol Oceanogr* 46(8):1945–1955.
31. Bassler BL, Gibbons PJ, Yu C, Roseman S (1991) Chitin utilization by marine bacteria. Degradation and catabolism of chitin oligosaccharides by *Vibrio furnissii*. *J Biol Chem* 266(36):24268–24275.
32. Seymour JR, Simó R, Ahmed T, Stocker R (2010) Chemoattraction to dimethylsulfoniopropionate throughout the marine microbial food web. *Science* 329(5989):342–345.
33. Blackburn N, Fenchel T, Mitchell J (1998) Microscale nutrient patches in planktonic habitats shown by chemotactic bacteria. *Science* 282(5397):2254–2256.
34. Kiørboe T, Jackson GA (2001) Marine snow, organic solute plumes, and optimal chemosensory behavior of bacteria. *Limnol Oceanogr* 46(6):1309–1318.
35. Azam F (1998) Microbial control of oceanic carbon flux: The plot thickens. *Science* 280(5346):694–696.
36. Mitchell JG, Okubo A, Fuhrman JA (1985) Microzones surrounding phytoplankton form the basis for a stratified marine microbial ecosystem. *Nature* 316(6023):58–59.
37. Fenchel T (2002) Microbial behavior in a heterogeneous world. *Science* 296(5570):1068–1071.
38. Charnov EL (1976) Optimal foraging, the marginal value theorem. *Theor Popul Biol* 9(2):129–136.
39. Kotler BP, Brown JS (2007) *Foraging: Behavior and Ecology*, eds Stephens DW, Brown JS, Ydenberg RC (Univ of Chicago Press, Chicago), pp 414–434.
40. Smith DC, Simon M, Alldredge AL, Azam F (1992) Intense hydrolytic enzyme-activity on marine aggregates and implications for rapid particle dissolution. *Nature* 359(6391):139–142.
41. Ahmed T, Shimizu TS, Stocker R (2010) Bacterial chemotaxis in linear and nonlinear steady microfluidic gradients. *Nano Lett* 10(9):3379–3385.
42. Tibbles BJ, Rawlings DE (1994) Characterization of nitrogen-fixing bacteria from a temperate saltmarsh lagoon, including isolates that produce ethane from acetylene. *Microb Ecol* 27(1):65–80.
43. Finster K, Tanimoto Y, Bak F (1992) Fermentation of methanethiol and dimethylsulfide by a newly isolated methanogenic bacterium. *Arch Microbiol* 157(5):425–430.